ADVANCED MATERIALS
www.advmat.de

Thermally Activated Delayed Fluorescent Dendrimers that Underpin High-Efficiency Host-Free Solution-Processed Organic Light-Emitting Diodes

Dianming Sun, Eimantas Duda, Xiaochun Fan, Rishabh Saxena, Ming Zhang, Sergey Bagnich, Xiaohong Zhang,* Anna Köhler,* and Eli Zysman-Colman**

The development of high-performance solution-processed organic light-emitting diodes (OLEDs) remains a challenge. An effective solution, highlighted in this work, is to use highly efficient thermally activated delayed fluorescence (TADF) dendrimers as emitters. Here, the design, synthesis, density functional theory (DFT) modeling, and photophysics of three triazine-based dendrimers, tBuCz2pTRZ, tBuCz2mTRZ, and tBuCz2m2pTRZ, is reported, which resolve the conflicting requirements of achieving simultaneously a small ΔE_{ST} and a large oscillator strength by incorporating both *meta*- and *para*-connected donor dendrons about a central triazine acceptor. The solution-processed OLED containing a host-free emitting layer exhibits an excellent maximum external quantum efficiency (EQE_{max}) of 28.7%, a current efficiency of 98.8 cd A^{-1}, and a power efficiency of 91.3 lm W^{-1}. The device emits with an electroluminescence maximum, λ_{EL}, of 540 nm and Commission International de l'Éclairage (CIE) color coordinates of (0.37, 0.57). This represents the most efficient host-free solution-processed OLED reported to date. Further optimization directed at improving the charge balance within the device results in an emissive layer containing 30 wt% OXD-7, which leads to an OLED with the similar EQE_{max} of 28.4% but showing a significantly improved efficiency rolloff where the EQE remains high at 22.7% at a luminance of 500 cd m^{-2}.

1. Introduction

Small-molecule-based thermally activated delayed fluorescence (TADF) materials[1] have proliferated since their first successful demonstration in high-efficiency organic light-emitting diodes (OLEDs).[2] A number of benchmark red,[3] green,[4] and blue[5] emitters have already been developed exhibiting more than 20% maximum external quantum efficiency, EQE_{max}, highlighting the significant and rapid advances in TADF materials' design and demonstrating their viability as replacement materials for state-of-the-art phosphorescent (for red and green) and fluorescent (blue) emitters in commercial OLEDs. However, the aforementioned high efficiency of the OLEDs relies not only on the intrinsic photophysical properties of the emitter but also on the rather complicated multilayered device architecture typically used in vacuum-deposited devices, which increases the cost of device fabrication. An alternative strategy would be to fabricate the OLED using lower-cost solution-processing techniques such as ink-jet printing.[6] TADF dendrimers are perfect candidates for solution-processed host-free OLEDs for the following reasons: 1) the singlet–triplet gap, ΔE_{ST}, can be easily adjusted within the modular molecular design using dendronized donors or acceptors; 2) intermolecular quenching can be largely avoided by careful design of the dendron motif; and 3) intersystem crossing (ISC) or reverse intersystem crossing

D. Sun, X. Fan, M. Zhang, X. Zhang
Institute of Functional Nano & Soft Materials (FUNSOM) and Jiangsu Key Laboratory for Carbon-Based Functional Materials & Devices
Joint International Research Laboratory of Carbon-Based Functional Materials and Devices
Soochow University
Suzhou, Jiangsu 215123, P. R. China
E-mail: xiaohong_zhang@suda.edu.cn

The ORCID identification number(s) for the author(s) of this article can be found under https://doi.org/10.1002/adma.202110344.

DOI: 10.1002/adma.202110344

D. Sun, E. Zysman-Colman
Organic Semiconductor Centre
EaStCHEM School of Chemistry
University of St Andrews
St Andrews KY16 9ST, UK
E-mail: sd235@st-andrews.ac.uk; eli.zysman-colman@st-andrews.ac.uk

E. Duda, R. Saxena, S. Bagnich, A. Köhler
Soft Matter Optoelectronics
BIMF & BPI
University of Bayreuth
Universitätsstraße 30, 95447 Bayreuth, Germany
E-mail: anna.koehler@uni-bayreuth.de

(RISC) rates can both be enhanced due to the large density of excited states.[7] Despite these identified advantages, to the best of our knowledge, only a handful dendrimer-based OLEDs have been reported. An overview of the history of the development of emissive dendrimers (pioneering work and state-of-the-art work for fluorescent, phosphorescent, and TADF dendrimers) is schematically outlined in **Figure 1**. The OLEDs using these dendrimers mostly show only moderate performance, with EQE_{max} ranging from 3% to 20%.[8]

The most widely used approach to construct a TADF dendrimer is to adopt a donor–acceptor design, one that is frequently used in small molecule TADF emitters, in which several donor dendrons (second, third, and fourth generations) are attached to a central acceptor by *para*-connected phenylene bridges.[8a] Efficient TADF can be achieved through delocalization of the highest occupied molecular orbital (HOMO) across increasing generations of donor dendrons.[9] However, the TADF performance of these dendrimers worsens because the electron coupling between dendrons and acceptor cores decreases with increasing dendrimer size beyond the second generation, resulting in significantly reduced oscillator strength, thus leading to a poorer photoluminescence quantum yield (PLQY). In order to mitigate aggregation-caused quenching (ACQ), the dendrimers must be dispersed at low concentrations within a suitable host matrix.[10] Another strategy is to decorate benchmark small TADF molecules with commonly used host units (e.g., mCP: 1,3-bis(*N*-carbazolyl)benzene, CBP: 4,4′-bis(*N*-carbazolyl)-1,1′-biphenyl, and TCTA: tris(4-carbazoyl-9-ylphenyl) amine) linked together by unconjugated alkyl chains.[8b,11] The performance of these dendrimers is directly dependent on the inherent properties of the TADF small-molecule-based core structures. The peripheral host dendrons are used to suppress concentration quenching and triplet–triplet annihilation (TTA) in pristine films. However, the device efficiencies employing these dendrimers remain generally inferior to those employing only the core small molecule TADF emitter when doped into a host matrix. There, thus, remains an outstanding challenge to design dendrimer-based emitters that show comparable efficiencies to their small molecule brethren.

Triphenyltriazine (TRZ) is one of the most common electron acceptors used in TADF emitter design. The D_3-symmetric structure permits up to three symmetric or asymmetric donor groups, or dendrons, to be attached to one TRZ moiety.[12] The first TADF dendrimers were designed based on trisubstituted second-to-fourth-generation carbazole-based donor dendrons grafted onto a central TRZ acceptor.[8a] Despite this design leading to extremely small ΔE_{ST} values (0.03–0.06 eV) due to a HOMO delocalized across the donor dendrons, the host-free OLEDs achieved an EQE_{max} of less than 5%. The performance of the "host-free" devices (EQE_{max} = 9.5%) could be improved by decorating each of the peripheral carbazoles with *tert*-butyl groups (tBuG2TAZ, cf., Figure 1).[8e] When this dendrimer was dispersed into a suitable host matrix, the EQE_{max} improved further to 16.1%. Overall, there is to date only a small number of examples of TADF emitters used in host-free OLEDs; of these, only a few reports document OLEDs with EQE_{max} superior to 20%, such as devices with **DMAC-TRZ**[13] (EQE_{max} = 20%, λ_{EL} = 500 nm), **DCB-BP-PXZ**[14] (EQE_{max} = 22.6%, λ_{EL} = 548 nm), and **DMAC-BPI**[15] (EQE_{max} = 24.7%, λ_{EL} = 508 nm). To date, the only dendrimer-based host-free solution-processed OLED with an EQE_{max} greater than 20% is that using **5CzBN-2Cz** as the emitter (EQE_{max} = 20.4%)[16] a hole-barrier layer of PO-T2T was, however, introduced into the device. These results illustrate the challenge of designing dendrimer emitters that can be used in high-performance host-free OLEDs.

2. Design of TADF Dendrimers

We initially designed two dendrimers, **tBuCz2pTRZ** and **tBuCz2mTRZ**, as reference molecules (Figure 1). These two dendrimers contain 3,3‴,6,6‴-tetrakis(*tert*-butyl-9″*H*-9,3″:6″,9‴-tercarbazole) (**tBuCz2G**) donors surrounding a triazine (TRZ) acceptor, linked either via a *para*-phenylene or a *meta*-phenylene bridge, respectively. We compared the optoelectronic properties of these model systems to the targeted emitter **tBuCz2m2pTRZ** (Figure 1), which is based on a design that combines facets of both **tBuCz2pTRZ** and **tBuCz2mTRZ**. We surmised that this design would inherit key properties from both dendrimers, with the excited-state behavior being modulated as a result of the interactions between the two adjacent donor dendrons. Our design follows three considerations: i) the *para*-connection of **tBuCz2pTRZ** leads to strong electronic coupling between the donor and the acceptor, which results in a high oscillator strength for the intramolecular charge-transfer (ICT) transition, while the *meta*-connection of **tBuCz2mTRZ** provides an avenue for an emitter possessing a small ΔE_{ST}, as the *meta*-disposed donor and acceptor groups are electronically decoupled. ii) The increasing number of peripheral dendritic moieties, the nature of how and the density with which they are packed together are expected to suppress quenching of the emission caused by intermolecular interactions. iii) The presence of many dendritic dendrons surrounding the central acceptor should lead to an increase in the density of triplet excited states that will enhance the nonadiabatic coupling to the singlet state thereby leading to more efficient RISC between T_1 and S_1.

We decided to focus only on a second-generation *tert*-butylcarbazole-based donor dendron as for most reported OLEDs using TADF dendrimers; the ones employing a second-generation donor dendron showed the highest EQE_{max}.[17] This observation is substantiated in our dendrimer design by density functional theory (DFT) calculations, which show that the oscillator strength decreases further due to the increased delocalization of HOMO when employing higher generations of donor dendrons (Figure S11, Supporting Information), implying reduced PLQY of higher generation dendrimers in our case.

Employing this strategy, a very small ΔE_{ST} (40 meV) coupled with a significant PLQY of 90% in solution has been realized simultaneously. Importantly, even as a pristine film, these excellent optoelectronic properties are conserved (ΔE_{ST} = 40 meV, PLQY = 86%). While the role of the *meta*- versus *para*-connection in the improvement of the electronic structure relevant to TADF is addressed in a related publication,[18] we focus here on the performance of the actual TADF devices. A host-free solution-processed OLED using a simple device configuration without exciton barrier layers and containing **tBuCz2m2pTRZ** as the emitter exhibited a record high EQE_{max} of 28.7%.

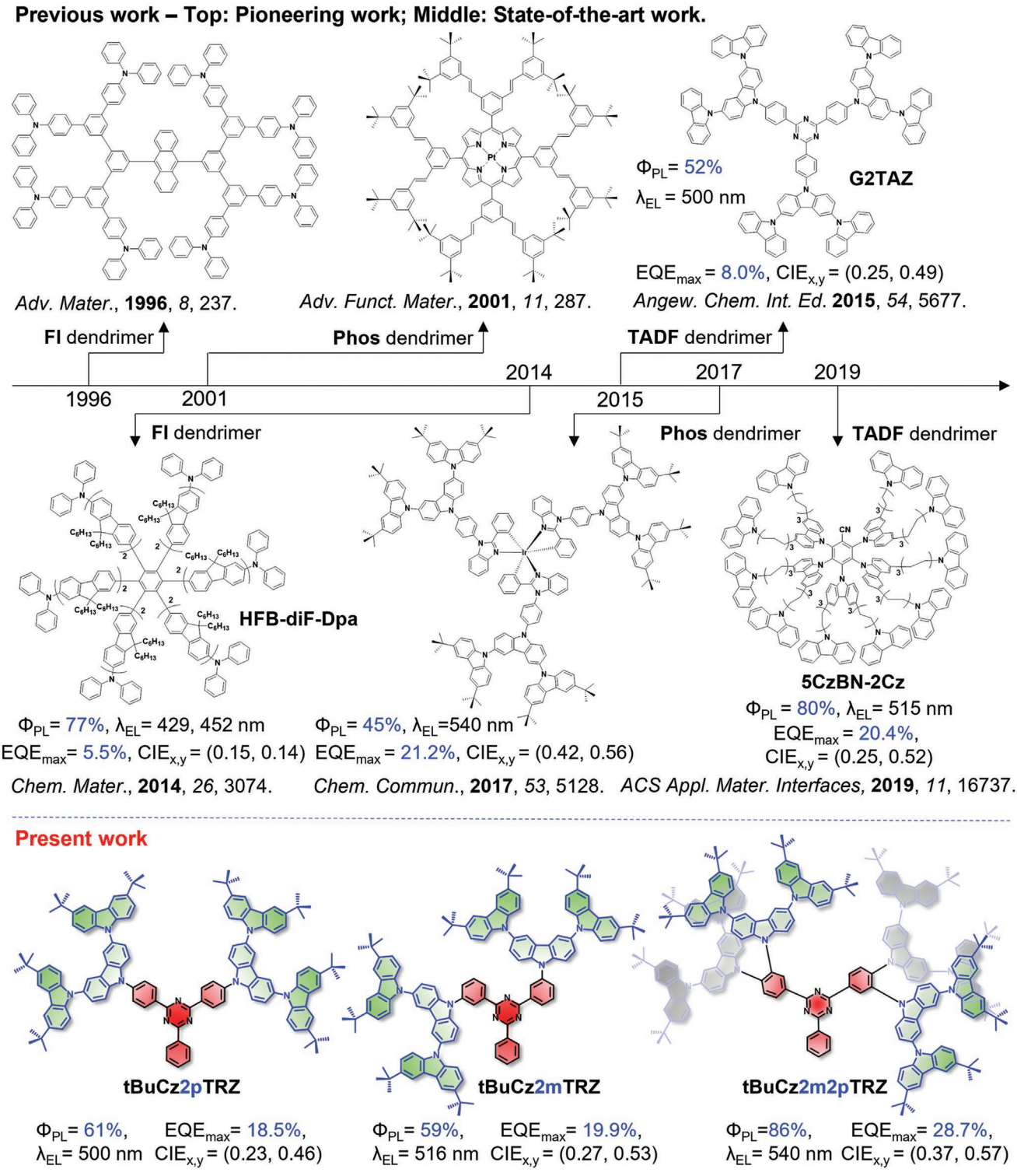

Figure 1. Molecular structures of pioneering work (top) and state-of-the-art work (middle) for fluorescent (Fl), phosphorescent (Phos), and TADF dendrimers used as emitters in OLEDs and structures of the dendrimers **tBuCz2pTRZ**, **tBuCz2mTRZ**, and **tBuCz2m2pTRZ** reported in this study (bottom) based on bespoke second-generation *tert*-butylcarbazole donor (**tBuCz2G**) and triphenyltriazine acceptor (TRZ) linked through *para*- and *meta*-connections.

Importantly, the efficiency roll-off of the OLED is significantly improved by doping 30 wt% OXD-7, an electron-transporting material, into the emissive layer. As a result of the improved charge balance, the EQE of the optimized device not only

reached a similar maximum EQE of 28.4%, but also maintained its efficiency of 22.7% at a luminance of 500 cd m^{-2}.

3. Theoretical Calculations

We started our investigation by employing quantum-chemical calculations to estimate the influence of the molecular design on both ΔE_{ST} and the oscillator strength, *f*, as well as to identify the hole and electron distributions in the lowest-lying excited singlet (S_1) and triplet states (T_1). **Figure 2**a displays the natural transition orbitals (NTOs) for S_1 and T_1. For all compounds, the hole and electron densities are clearly separated. Complemented by a solvatochromic study (Figure 2b), and as discussed further in the following sections, all spectra can be ascribed to charge-transfer (CT) transitions. Even though all three compounds show the same negligible wavefunction overlap, significant differences in the calculated oscillator strength exist. While **tBuCz2pTRZ** has the largest calculated oscillator strength ($f = 0.26$), it is negligible for **tBuCz2mTRZ** ($f = 0.002$). The significantly higher oscillator strength calculated for **tBuCz2pTRZ** in the gas phase is expected due to a stronger electronic coupling between donor dendrons and the TRZ acceptor through the *para*-connection compared to the *meta*-connection in **tBuCz2mTRZ**. In the case of **tBuCz2m2pTRZ** ($f = 0.10$), the oscillator strength is of an intermediate intensity to those of **tBuCz2pTRZ** and **tBuCz2mTRZ**. The calculations show that the ΔE_{ST} values are about equal

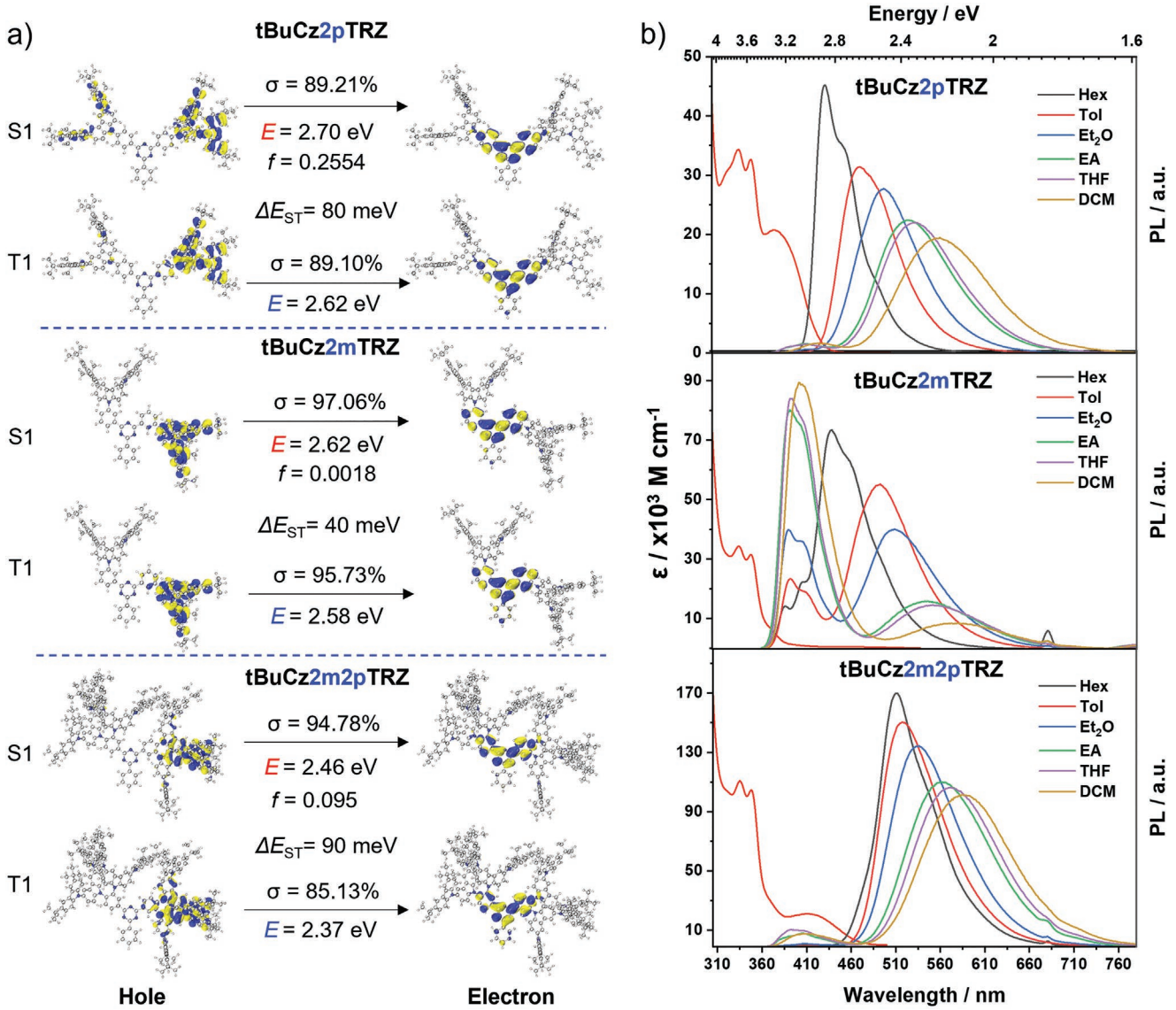

Figure 2. Theoretical and photophysical properties of **tBuCz2pTRZ** (top), **tBuCz2mTRZ** (middle), and **tBuCz2m2pTRZ** (bottom). a) Pictorial representation of the natural transition orbitals (NTO) describing the S_1 and T_1 states for **tBuCz2m2pTRZ**, as calculated at the TDA-PBE0/6-31G(d,p) level (isovalue = 0.02) where σ refers to the weight of the illustrated hole–electron contribution to the excitation, and *f* indicates the oscillator strength, and E_{S1} and E_{T1} are the calculated lowest singlet and triplet excited states, respectively. b) Molar absorptivity measured in toluene and solvatochromic PL spectra normalized by the integrated area ($\lambda_{exc} = 340$ nm; 3×10^{-5} M). (The emission at 680 nm arises from the second harmonic of the laser source.)

(80 and 90 meV) for **tBuCz2pTRZ** and **tBuCz2m2pTRZ**, but half as large as 40 meV for **tBuCz2mTRZ**.

The optimized structures in the ground state and the electron density distributions of the HOMO and lowest unoccupied moleular orbital (LUMO) of **tBuCz2pTRZ**, **tBuCz2mTRZ**, and **tBuCz2m2pTRZ** are shown in Figures S3 and S4 (Supporting Information) (calculated at the PBE0/6-31G(d,p) level). The TRZ acceptor within each dendrimer adopts a nearly planar conformation. The dihedral angle between the planes of the inner carbazoles, and the TRZ values are similar at around 55° and 53° for **tBuCz2pTRZ** and **tBuCz2mTRZ**, respectively. Interestingly, although large steric repulsion exists between *para*- and *meta*-connected donor dendrons in **tBuCz2m2pTRZ**, the conformations of the donor dendrons in the model dendrimers are conserved, with dihedral angles (54° for *para*-connections and 55° for *meta*-connections) that are similar to those in **tBuCz2pTRZ** and **tBuCz2mTRZ**. This indicates that the degree of conjugation observed in **tBuCz2pTRZ** and **tBuCz2mTRZ** will be maintained in **tBuCz2m2pTRZ**.

Furthermore, calculations show that there are corresponding degenerate S_2 and T_2 states due to the symmetry of the molecular structures. The DFT calculations also reveal the presence of multiple excited states arising from CT transition of donor dendron (D) to the TRZ acceptor (A) for **tBuCz2pTRZ**, **tBuCz2mTRZ**, and **tBuCz2m2pTRZ** (see Tables S2–S4 in the Supporting Information). We expect that these higher-lying CT states will show substantial mixing with the lowest ^{1,3}CT states by both spin–orbit coupling (SOC) and spin–vibronic coupling. The large number of closely lying excited states should directly translate into faster ISC and RISC rates in an analogous fashion to how D–A–D TADF emitters show more efficient TADF and higher PLQY compared to their D–A analogs.[7a,19] This aspect is addressed in more detail in a study on the difference between the electronic structure of the *meta*- and *para*-connected compounds.[18]

4. Electrochemistry

For solution-processed OLEDs, an emitting layer (EML) is generally spin-coated onto a wet-processed poly(3,4-ethylenedioxythiophene):poly(styrenesulfonate) (PEDOT:PSS) hole injection layer without any additional hole-transporting material, in part because spin-coating of the EML may dissolve/disturb the underlying hole-transporting layer. A relatively high-lying HOMO energy level is required for the emitters to match the HOMO level of PEDOT:PSS (–5.1 eV)[20] and thus ensure efficient hole injection. As shown in Figure S4 (Supporting Information), all three dendrimers possess similar electrochemical properties, with two resolvable quasireversible oxidation waves with E_{ox} at 1.07 and 1.19 eV versus saturated calomel electrode (SCE) (measured from the peak value of the differential pulse voltammetry (DPV) scan), which correspond to the oxidation of the inner carbazole and the peripheral *tert*-butylcarbazole, respectively.[21] Scanning to negative potentials, the E_{red} (measured from the peak value of the DPV scan) of –1.54 V versus SCE for **tBuCz2m2pTRZ** is anodically shifted by 0.13 V compared to those of **tBuCz2pTRZ** and **tBuCz2mTRZ**, both of which show the same E_{red} of –1.67 V versus SCE. This shift is consistent with a slightly greater conjugation between the acceptor and two additional **tBuCz2G** dendrons in **tBuCz2m2pTRZ** as evidenced by the DFT calculations (see Figure 2a). Thus, in summary, the HOMO levels are –5.41 eV for all three dendrimers while the LUMO levels are –2.67, –2.67, and –2.8 eV for **tBuCz2pTRZ**, **tBuCz2mTRZ**, and **tBuCz2m2pTRZ**, respectively.

5. Photophysical Properties

To exclude bimolecular interactions and to assess the properties of monomolecular species, we started the photophysical investigation with absorption and photoluminescence measurements in dilute solution. In Figure 2b, the absorption spectra for all three compounds in toluene show very similar profiles. Peaks at λ_{abs} = 337 and 342 nm can be ascribed to the π–π^* transitions on the carbazole.[22] The broad band at 385 nm for **tBuCz2pTRZ** is assigned to an ICT transition from the *para*-connected donor dendron to the TRZ acceptor with a molar extinction coefficient, ε = 3500 M^{-1} cm^{-1}; a weak ICT absorption (ε = 300 M^{-1} cm^{-1}) is barely visible for **tBuCz2mTRZ**. In contrast, as shown in Figure 2b (top and bottom), the ICT absorption for **tBuCz2m2pTRZ** at 415 nm (ε = 1500 M^{-1} cm^{-1}) is comparable to that of **tBuCz2pTRZ**, consistent with the *para*-connected donor dendrons that contribute to the large oscillator strength; further, it is redshifted, in line with the trends in the electrochemical gaps observed by DPV (Figure S4, Supporting Information). While the gas phase calculations suggest an increase of factors of 100 and 50, respectively, for the oscillator strength when going from the *meta*-connected compound **tBuCz2mTRZ** to the compounds with *para*-connected carbazoles, **tBuCz2pTRZ** and **tBuCz2m2pTRZ**, the solution measurements yield a much weaker increase of only factors of 7 and 3, respectively. We attribute this to conformational deviations from the perfect gas phase geometry in solution due to the presence of the solvent molecules that reduce the maximal possible excited state delocalization.

Figure 2b shows the photoluminescence spectra of the three compounds in a range of solvents of increasing polarity ($f(\varepsilon,n)$ = 0, 0.013, 0.167, 0.200, 0.210, and 0.217 for hexane, toluene, diethyl ether, EtOAc, tetrahydrofuran (THF), and dichloromethane (DCM), respectively;[23] $f(\varepsilon,n)$ is a solvent polarity function). Two emission bands can be identified. With increasing solvent polarity, the emission peak of the high-energy band retains its spectral position around 400 nm while the low-energy band redshifts to longer wavelength and the emission band broadens. This positive solvatochromism of the low-energy band is typical for an ICT state. Due to the absence of spectral shift with increasing solvent polarity, the high-energy band can be associated with a locally excited (LE) state. The relative intensity of this LE band is low when a *para*-connection is present, i.e., for **tBuCz2pTRZ** and **tBuCz2m2pTRZ** (see Figure S14 in the Supporting Information for the log scale). For **tBuCz2mTRZ**, where only a *meta*-connection exists, the relative intensity of the LE band increases with increasing solvent polarity and, thus, energetic separation from the CT state. This is straightforward to understand. Simultaneous emission from an LE and a CT state can be observed when internal conversion from the LE to the CT state is slower than radiative decay from the LE state.

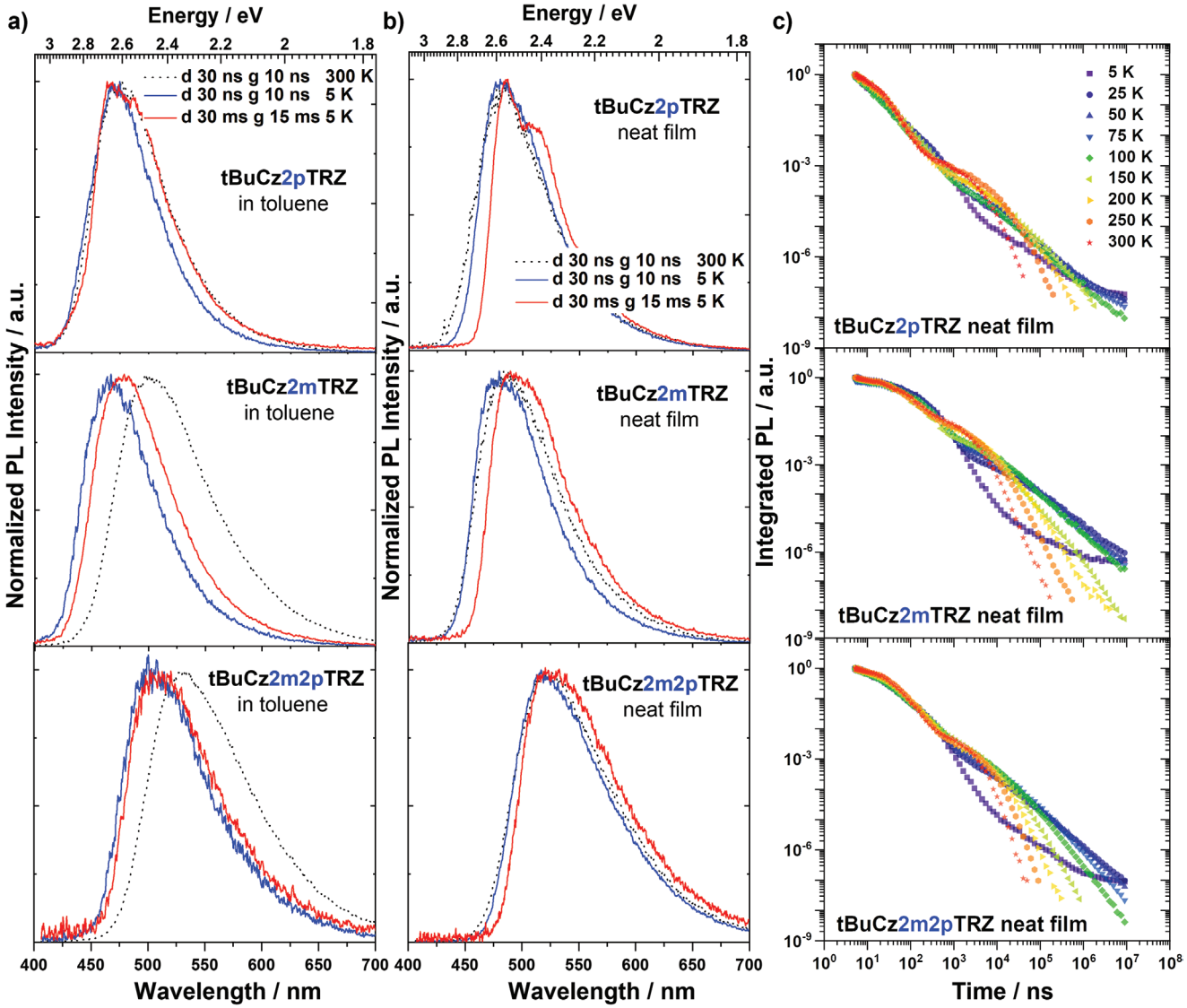

Figure 3. Prompt fluorescence ($d = 30$ ns g^{-1}: 10 ns) at 300 K (black dotted line) and at 5 K (blue solid line). a,b) Phosphorescence with detection in the millisecond range ($d = 30$ ms g^{-1}: 15 ms) at 5 K (red solid line) of **tBuCz2pTRZ** (top), **tBuCz2mTRZ** (middle), and **tBuCz2m2pTRZ** (bottom) in 3×10^{-5} M toluene solution (a) and neat film (b). In the legend, *d* refers to delay time and *g* refers to gate time. c) Temperature-dependent time-resolved PL decay of neat films. The decays were obtained by integrating each time-resolved spectrum across the full spectral range ($\lambda_{exc} = 355$ nm).

The conversion from an LE to a CT state implies an electron transfer, which depends strongly on the wavefunction overlap. This should, therefore, be faster for the compounds with *para*-connected donor dendrons than with *meta*-connected donor dendrons, consistent with a greater relative CT emission. There are two further factors that contribute to the ratio of LE:CT emission. First, with increasing polarity, the CT character in the CT state increases and this reduces its emission intensity, so that the relative contribution from the LE state emission gains weight. Further, the internal conversion rate slows with an increasing gap between the two states, known as the energy gap law, implying more LE emission in the more polar solvents, where the gap between LE and CT states is larger. Overall, the simultaneous LE and CT state emission indicates that, for some of the donor dendrons, the rate of ICT is slow compared to the radiative emission rate from the LE state. These groups could therefore act as hole-transporting units or host moieties, given their suitably higher triplet energies for the ICT-based emission of the dendrimers.

Prompt and delayed emissions were measured after pulsed excitation in order to gain deeper insight into the nature of the excited states of the emitters in solution and film. **Figure 3**a shows the prompt spectra of the three dendrimers in 3×10^{-5} M toluene solution with a delay time of 30 ns and a gating time of 10 ns. The characteristically broad and unstructured prompt emission in toluene, corroborated by quantum-chemical calculations (Figure 2; Figures S8–S10, Supporting Information), indicate strong CT character for all three dendrimers. The prompt emission at both 300 and 5 K is almost identical for **tBuCz2pTRZ**, while in contrast, there exists a significant blueshift upon cooling from 300 to 5 K for **tBuCz2mTRZ** and **tBuCz2m2pTRZ**, both of which contain electronically

decoupled donor dendrons. The blueshift is due to reduced geometric reorganization after excitation at 5 K because of the rigid matrix. The singlet energies were then measured from the onset of the prompt emission spectra at 5 K to be 2.92, 2.94, and 2.73 eV for **tBuCz2pTRZ**, **tBuCz2mTRZ**, and **tBuCz2m2pTRZ**, respectively (see Figure S15 in the Supporting Information); if the central peak positions are taken, the respective values are 2.64, 2.66, and 2.48 eV. The singlet energies of **tBuCz2pTRZ** are nearly isoenergetic to those of **tBuCz2mTRZ**, indicating similar energies of their lowest singlet (^{1}CT) states regardless of the electronic coupling between the donor and acceptor. The spectra determined at 5 K using a long delay time of 30 ms (gate time = 15 ms) are ascribed to phosphorescence. Similar to the prompt emission, the phosphorescence spectra are also broad and structureless, indicating emission from ^{3}CT states, assignments that are also supported by quantum-chemical calculations (Figures S8–S10, Supporting Information). The phosphorescence spectrum of **tBuCz2mTRZ** closely resembles that of **tBuCz2pTRZ**, resulting in close-lying triplet states at 2.83 and 2.88 eV, for **tBuCz2pTRZ** and **tBuCz2mTRZ**, respectively, measured from the onset of these spectra. Taking the offset between the prompt emission and phosphorescence spectra, ΔE_{ST} values of 90 and 60 meV were estimated for **tBuCz2pTRZ** and **tBuCz2mTRZ**, respectively. The T_1 state of **tBuCz2m2pTRZ** has its onset at 2.69 eV, leading to a ΔE_{ST} value of 40 meV. The presence of the smaller gap between the singlet and triplet states should lead to faster RISC in this dendrimer. The estimated ΔE_{ST} values agree largely with the quantum-chemical calculations.

For electroluminescent devices, it is essential to understand how the photophysical properties in solution translate into neat films. In the context of host-free devices, we therefore next investigated the neat thin-film photophysics of **tBuCz2pTRZ**, **tBuCz2mTRZ**, and **tBuCz2m2pTRZ** at 300 and at 5 K (Figure 3b). Similar to the features observed in toluene, the prompt emission at both 300 and 5 K in neat films is also broad and unstructured. However, in neat films, the prompt emission at 300 K resembles that at 5 K for each dendrimer, unlike that observed for the prompt emission behavior of **tBuCz2mTRZ** and **tBuCz2pTRZ** in toluene. This implies that there is little reorganization after excitation within the thin film even at room temperature (RT) due to the packing of the emitters within the film. The prompt emission of **tBuCz2pTRZ** still closely resembles that of **tBuCz2mTRZ**. The energy levels of the ^{1}CT states determined from the onsets of the corresponding prompt fluorescence (PF) spectra at 5 K are calculated to be 2.78, 2.81, and 2.63 eV for **tBuCz2pTRZ**, **tBuCz2mTRZ**, and **tBuCz2m2pTRZ**, respectively, values that are stabilized by 140–160 meV compared to those in toluene glass. The spectra obtained at 5 K after a time delay of 30 ms are, again, ascribed to phosphorescence. The phosphorescence spectrum for **tBuCz2pTRZ** is structured with a major peak at 486 nm (2.55 eV) and a low energy feature around 510 nm (2.43 eV) that we ascribe to unresolved vibrational transition. The phosphorescence spectra of **tBuCz2mTRZ** and **tBuCz2m2pTRZ** remain unstructured and broader than the phosphorescence spectrum of **tBuCz2pTRZ**, which we ascribe to a more significant structural disorder due to the presence of the *meta*-connected donor dendron, and, for **tBuCz2m2pTRZ**, a greater number of dendrons. The energies of the T_1 states of **tBuCz2pTRZ** and **tBuCz2mTRZ** measured from the onsets are 2.69 and 2.72 eV, respectively, leading to the same ΔE_{ST} value of 90 meV. The similar energies of their respective S_1 and T_1 states indicate that the presence of *para*- or *meta*-connections between the donor and acceptor has only a small effect on the nature of the excited states. The energy of the T_1 state of **tBuCz2m2pTRZ** is located at 2.59 eV, leading to the smallest ΔE_{ST} value of 40 meV, which is also the same value as that determined in toluene glass.

Figure 3c shows the PL decay curves of neat films. All decays at 300 K show two regimes, a PF regime followed by a delayed fluorescence (DF) component from about 500 ns onward. The intensity of DF decreases upon cooling and vanishes at 5 K, yet, for **tBuCz2mTRZ** and **tBuCz2m2pTRZ**, most thermal activation occurs between 5 and 25 K (Figures S18 and S19, Supporting Information), implying a very efficient RISC even at low temperature. The corresponding activation energies for **tBuCz2mTRZ** and **tBuCz2m2pTRZ** are likely to be smaller than the optical ΔE_{ST} determined from the difference in offsets of the prompt fluorescence and phosphorescence spectra at 5 K. Part of the fast RISC rate can be accounted for by the large number of higher-lying excited states, as predicted by the quantum-chemical calculations.[7a,24]

The PLQY values of the neat films as well as other photophysical parameters are collated in **Table 1**. Under N_2, **tBuCz2pTRZ** and **tBuCz2mTRZ** have similar PLQY values of 61% and 59%, respectively. For **tBuCz2m2pTRZ**, the PLQY in

Table 1. Comparison of photophysical properties in neat films at 300 K.

Neat film	λ_{PL}[a] [nm]	S_1[b] [eV]	T_1[c] [eV]	ΔE_{ST}[d] [eV]	Φ_{PL} N_2[e] [%]	τ_{PF}[f] [ns]	τ_{DF}[g] [μs]	DF/PF[h]	k_{PF}[i] [$\times 10^7$ s^{-1}]	k_{DF}[j] [$\times 10^5$ s^{-1}]	k_r^S[k] [$\times 10^7$ s^{-1}]	k_{nr}[l] [$\times 10^7$ s^{-1}]
tBuCz2pTRZ	481	2.78	2.69	0.09	61	11	1.2	0.15	9.1	8.3	4.8	4.3
tBuCz2mTRZ	483	2.81	2.72	0.09	59	52	1.1	1.3	1.9	9.1	0.5	1.4
tBuCz2m2pTRZ	520	2.63	2.59	0.04	86	31	1.1	0.4	3.2	9.1	2.0	1.2

[a] PL in neat film at 300 K; [b] Lowest singlet energy; [c] Lowest triplet energy; [d] Energy difference between S_1 and T_1; [e] Photoluminescence quantum yield; [f] Lifetime of prompt emission (obtained by single exponential fitting of prompt emission decay regime at RT as shown in Figure S20 (Supporting Information)) λ_{exc} = 355 nm; [g] Lifetime of delayed emission (obtained by single exponential fitting of delayed emission decay regime at RT as shown in Figure S20 (Supporting Information)) λ_{exc} = 355 nm; [h] $DF/PF = \int \frac{I_{DF(t)}}{I_{PF(t)}} dt$; [i] Decay rate of prompt emission; [j] Decay rate of delayed emission; [k] Radiative decay rate of singlet excitons; [l] Nonradiative decay rate determined by $\Phi_{PF} = \frac{k_r^S}{k_r^S + k_{nr}}$.

N_2 is the highest among three dendrimers at 86%. To evaluate this in view of the TADF performance, the respective rates should be considered. First, the nonradiative rate reduces by a factor of 3 in the *meta*-connected compounds, **tBuCz2mTRZ** and **tBuCz2m2pTRZ**. The dominant nonradiative decay channel will be intersystem crossing; since we are in the blue-green spectral range, internal conversion is negligible, and the similar photoluminescence quantum yields in solution and neat film indicate that intermolecular interactions leading to concentration quenching are small. Further, even though the ISC rate is three times reduced, the RISC rate is 3–5 times faster in the two compounds with *meta*-connection (Table S7, Supporting Information). In an OLED structure, the triplet states are populated directly by hole–electron recombination, so that the ISC from S_1 to T_1 is not relevant, yet the RISC from T_1 to S_1 is decisive. This clearly places the compounds with *meta*-connections ahead of the *para*-connected one. For **tBuCz2m2pTRZ**, the radiative decay rate is about half that of the *para*-connected **tBuCz2pTRZ**, yet still four times greater than that of the purely *meta*-connected **tBuCz2mTRZ**. It seems that **tBuCz2m2pTRZ** embodies the best of both RISC and radiative decay rates from the *meta*- and the *para*-connected compounds. Notably, the lifetime of the delayed emission is very short for all three compounds, as desired for an emitter in an OLED (Table 1).

6. OLEDs

Motivated by the promising photophysical properties, we next fabricated devices. First, single carrier devices containing neat EMLs with **tBuCz2pTRZ**, **tBuCz2mTRZ**, and **tBuCz2m2pTRZ** were fabricated with the configuration of indium tin oxide (ITO)/PEDOT:PSS (35 nm)/dendrimer (40 nm)/MoO_3 (40 nm)/Al (100 nm) for hole-only devices and ITO/Al (40 nm)/dendrimer (40 nm)/TmPyPB (40 nm)/LiF (1 nm)/Al (100 nm) for electron-only devices, where TmPyPB is 1,3,5-tri(*m*-pyrid-3-yl-phenyl)benzene and acts as an electron-transporting layer. Their current density–voltage (*J*–*V*) characteristics are shown in Figure S22 (Supporting Information). The hole current starts to rise at a low threshold voltage of 3 V whereas electron current grows rapidly at around 5 V for all three devices, indicative of similar hole/electron injection barriers and efficient hole injection character of the three dendrimers. For hole-only devices with Ohmic electrodes, a higher hole current density at the same driving voltage indicates a better hole mobility. Thus, the hole-transporting ability follows the order of **tBuCz2pTRZ** < **tBuCz2mTRZ** < **tBuCz2m2pTRZ**. By contrast, similar electron-transporting/injection ability is observed for all three dendrimer devices as evidenced by the nearly identical electron current density curves. This is not unexpected given that all three dendrimers possess the same TRZ acceptor unit. Importantly, at the same effective driving voltage for both hole-only and electron-only devices, the electron currents in the electron-only devices are higher than the hole currents in the hole-only devices, indicating improved electron-transporting properties within the EML. We surmise that this is due to the presence of a similarly exposed TRZ in each dendrimer that provides an efficient pathway for electron transport.

We next fabricated simple bilayer devices consisting of ITO/PEDOT:PSS (35 nm)/dendrimer (40 nm)/TmPyPB (40 nm)/LiF (1 nm)/Al (100 nm). The emissive layer is composed of a neat film of one of **tBuCz2pTRZ**, **tBuCz2mTRZ**, and **tBuCz2m2pTRZ** for devices 1–3, respectively. The schematic diagram of the device structure together with energy level of each layer is shown in **Figure 4**a. The device performance is summarized in **Table 2**. The electroluminescence (EL) spectra of the devices are presented in Figure 4b. The EL spectra gradually redshift from devices 1 to 3, which is consistent with the trends observed for the PL spectra in toluene and as neat films. Device 3 is green emissive with a λ_{EL} of 540 nm and Commission Internationale de L'Éclairage (CIE) coordinates of (0.37, 0.57).

Figure 4c shows the current density–voltage–luminance (*J*–*V*–*L*) curves for these devices, all of which exhibit low turn on voltages between 3.1 and 3.3 V that are among the lowest values reported for solution-processed TADF OLEDs (see Table S8 in the Supporting Information). As a result, excellent power efficiencies, as high as 91.3 lm W^{-1} for the host-free device based on **tBuCz2m2pTRZ**, were reached. Among all these devices, the **tBuCz2m2pTRZ**-based device 3 shows the highest luminance of 6029 cd m^{-2} at 6.3 V, whereas device 1 achieved only half of that value and device 2 achieved only 777 cd m^{-2}.

Figure 4d shows the EQE versus current density for these devices. The EQE_{max} of the best-performing examples of devices 1–3 are 18.5%, 19.9%, and 28.7%, respectively. The EQE_{max} of device 3 is obtained at a luminance of 40 cd m^{-2}. The performance of device 3 is significantly improved compared to those of the other two OLEDs. Notably, the average EQE_{max} values across 20 fabricated devices are 16.8%, 15.8%, and 26.3% for devices 1–3, respectively, according to the histogram of EQE_{max} values (Figure 4e). The average EQE_{max} of 26.3% for **tBuCz2m2pTRZ** is close to the highest obtained EQE_{max} (28.7%), indicating high batch-to-batch reproducibility.

However, we do note the severe efficiency roll-off for device 3, which shows an EQE of 14.3% at 500 cd m^{-2}, which we ascribe to the imbalanced charge mobility within the **tBuCz2m2pTRZ** neat film. To address this issue, we doped into the emissive layer OXD-7 at 30 wt%, which serves as an electron-transporting material (**Figure 5**). Device 4, containing the OXD-7, shows the same low turn-on voltage at 3.1 V and the EL spectrum also remains the same. Device 4 shows a comparable EQE_{max} of 28.4% to device 3. Importantly, a significant improvement in efficiency roll-off is observed for device 4 where the EQE reaches 22.7% at a luminance of 500 cd m^{-2} (Figure 5d). These champion values imply very effective exciton harvesting of **tBuCz2m2pTRZ** in the OLEDs, and concentration quenching that is largely suppressed in both devices 3 and 4. The extremely small ΔE_{ST}, very fast RISC, and the intermolecular packing of the dendrimers account for the significant improvement in performance compared to OLEDs using previously reported TADF dendrimers.

7. Conclusions

By taking advantage of the molecular design features embedded within **tBuCz2m2pTRZ**, we have rationalized the remarkable improvement in photophysical properties and device

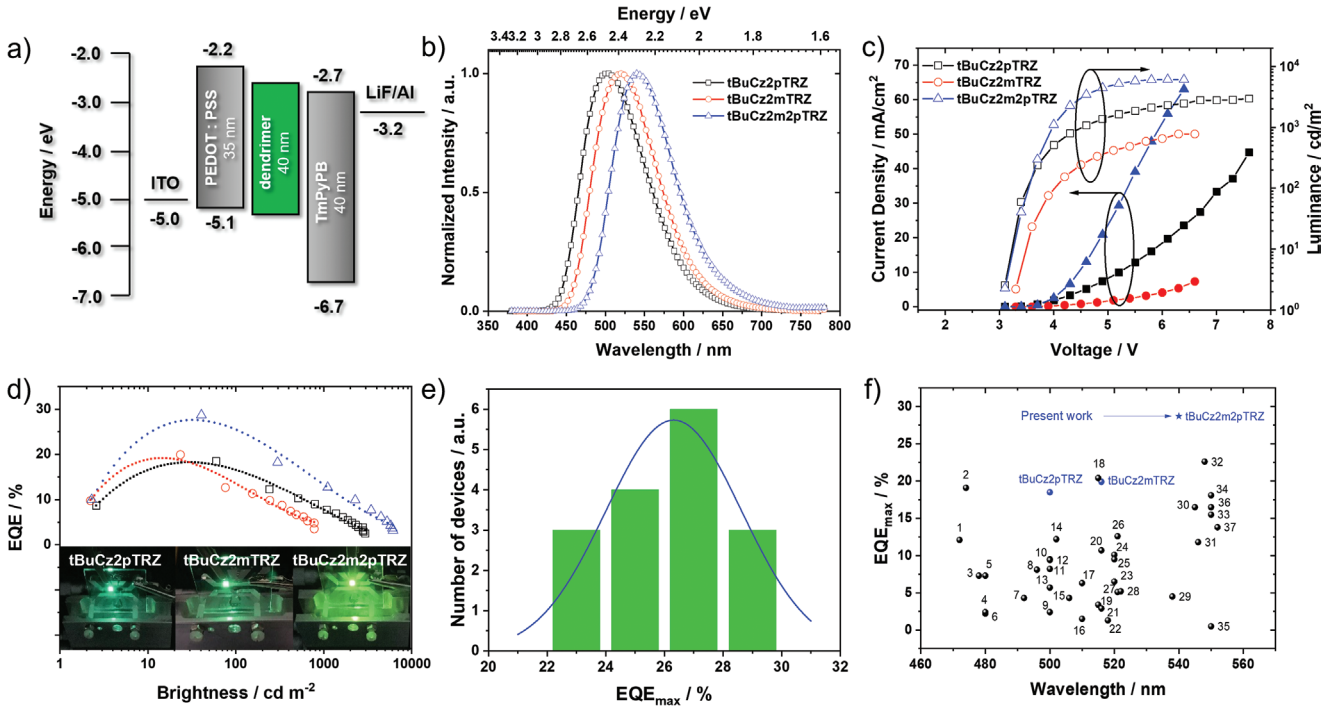

Figure 4. Electroluminescence characteristics of host-free OLEDs using **tBuCz2pTRZ**, **tBuCz2mTRZ**, and **tBuCz2m2pTRZ** as emitters. a) Device configuration. b) Normalized electroluminescence spectra. c) Current density and luminance versus driving voltage characteristics. d) EQE versus brightness for **tBuCz2pTRZ**-based (black), **tBuCz2mTRZ**-based (red), and **tBuCz2m2pTRZ** (blue)-based devices (the photos shown from bottom left to right are for **tBuCz2pTRZ-**, **tBuCz2mTRZ-**, and **tBuCz2m2pTRZ**-based devices, respectively). e) Statistical histogram of EQE_{max} for **tBuCz2m2pTRZ-**based OLEDs. f) The EQE_{max} of all reported solution-processed host-free TADF OLEDs as a function of wavelength. All the data for devices are summarized in Table S8 (Supporting Information).

performance through the synergistic effects of *meta*- and *para*-connected donor dendrons to the central triazine acceptor core. Importantly, there are a large number of low-lying excited states in **tBuCz2m2pTRZ** that facilitates reverse intersystem crossing, and the distribution of donor dendrons can effectively suppress concentration quenching. The photophysical investigation in solution also indicates that some dendrons, which have very slow internal charge transfer, may be able to function as host moieties. The extremely small ΔE_{ST} and large oscillator strength in both solution and neat film are evidence of the qualities that make **tBuCz2m2pTRZ** a high-performance emitter in efficient solution-processed OLEDs. We believe that the dendrimer design strategy disclosed in our study provides a route to high-performance solution-processed TADF OLEDs and evidences the full potential of dendrimers as emissive materials.

8. Experimental Section

Synthesis: The procedures for the synthesis of the TADF dendrimer and the corresponding characterization are reported in the Supporting Information.

Sample Preparation and Photophysical Characterization: All solution samples were prepared in high-performance liquid chromatography (HPLC) grade solvents with varying concentrations on the order of 10^{-5} or 10^{-6} M for absorption and emission studies. Films were prepared by spin-coating 10 mg mL^{-1} of chloroform solutions of dendrimers. Absorption spectra were recorded at RT using a Shimadzu UV1800 double-beam spectrophotometer. Steady-state emission spectra and phosphorescence spectra were obtained using a Jasco FP-8600 spectrofluorometer. The time-resolved emission measurements were obtained using the iCCD camera by exponentially increasing delay and gating times where the gating time was kept lower by ten times compared to the delay time. All measurements were recorded under vacuum unless otherwise stated. Full details are presented in the Supporting Information.

Table 2. Summary of device performance.

Device No.[a)]	Emitting layer	λ_{EL} [nm]	FWHM[b)] [nm]	V_{on}[c)] [V]	CE_{max} [cd A^{-1}]	PE_{max} [lm W^{-1}]	EQE_{max} [%]	EQE_{100} [%]	EQE_{500} [%]	CIE (*x*,*y*)
1	**tBuCz2pTRZ**	500	95	3.1	49.4	45.7	18.5	16.1	10.3	0.23, 0.46
2	**tBuCz2mTRZ**	516	95	3.3	59.9	52.2	19.9	12.0	6.4	0.27, 0.53
3	**tBuCz2m2pTRZ**	540	97	3.1	98.8	91.3	28.7	21.2	14.3	0.37, 0.57
4	**tBuCz2m2pTRZ+ 30 wt% OXD-7**	540	97	3.1	95.4	88.1	28.4	26.4	22.7	0.37, 0.57

[a)]The device structure is ITO/PEDOT:PSS (35 nm)/dendrimer (40 nm)/TmPyPB (40 nm)/LiF (1 nm)/Al (100 nm); [b)]Full wavelength at highest maximum; [c)]At the luminance of 1 cd m^{-2}.

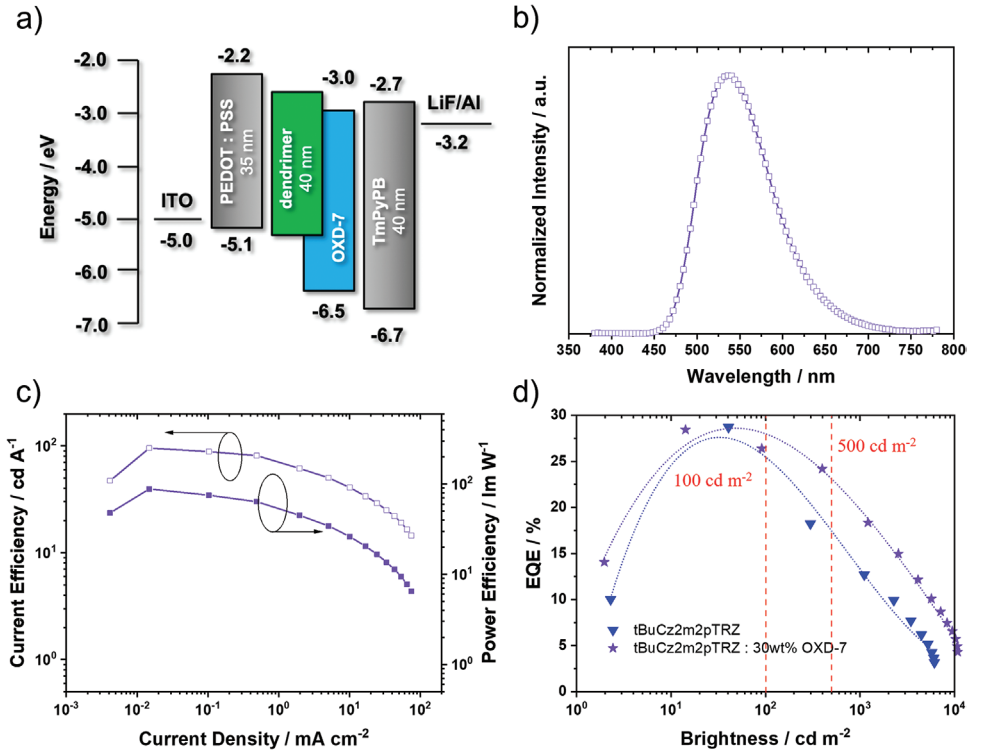

Figure 5. Electroluminescence characteristics of the OLED based on a **tBuCz2m2pTRZ**:30 wt% OXD-7 EML. a) Device configuration. b) Normalized electroluminescence spectra. c) Current efficiency and power efficiency versus current density. d) EQE versus brightness (comparison with the device without doping OXD-7 in the EML).

OLED Fabrication: The OLED devices were fabricated using a bottom-emitting architecture. A prepatterned ITO glass substrate was used as the anode. PEDOT:PSS8000 was spin-coated onto the clean ITO substrate as a hole-injection layer, then the 10 mg mL^{-1} dendrimers in chlorobenzene solution were spin-coated to form the EML. TmPyPB, LiF, and Al were each subsequently vacuum-deposited onto EML. More details are shown in the Supporting Information.

Supporting Information

Supporting Information is available from the Wiley Online Library or from the author.

Acknowledgements

D.S. and E.D. contributed equally to this work. This project received funding from the European Union's Horizon 2020 research and innovation program under the Marie Skłodowska–Curie grant agreements (Grant Nos. 838009 (TSFP) and 812872 (TADFlife). D.S. acknowledges support from the Marie Skłodowska-Curie Individual Fellowship (TSFP), the National Postdoctoral Program for Innovative Talents (Program No. BX201700164), and the Jiangsu Planned Projects for Postdoctoral Research Funds (Project No. 2018K011A). S.B. acknowledges support from the German Science Foundation (Grant No. 392306670/HU2362). The St Andrews team thank the Leverhulme Trust (RPG-2016047) and EPSRC (EP/P010482/1) for financial support. The authors thank Umicore AG for the gift of materials. X.Z. would like to thank the support from the National Key Research & Development Program of China (Grant Nos. 2020YFA0714601 and 2020YFA0714604), the National Natural Science Foundation of China (Grant Nos. 52130304 and 51821002), Suzhou Key Laboratory of Functional Nano & Soft Materials, Collaborative Innovation Center of Suzhou Nano Science & Technology, the Priority Academic Program Development of Jiangsu Higher Education Institutions (PAPD), the 111 Project, Joint International Research Laboratory of Carbon-Based Functional Materials and Devices. E.Z.-C. is a Royal Society Leverhulme Trust Senior Research fellow (SRF\R1\201089).

Conflict of Interest

Dr. Dianming Sun and Prof. Eli Zysman-Colman are the co-inventors of a patent, PCT/GB2021/052844, based on the materials in this manuscript.

Data Availability Statement

The research data supporting this publication can be accessed at the University of St Andrews' Research Portal at https://doi.org/10.17630/e24f7f28-a9b4-426d-a74ff37334f08a0b.

Keywords

carbazole, external quantum efficiency, host-free organic light-emitting diodes, solution-processing, thermally activated delayed fluorescence dendrimers

Received: December 19, 2021
Revised: March 14, 2022
Published online:

[1] a) Y. Tao, K. Yuan, T. Chen, P. Xu, H. Li, R. Chen, C. Zheng, L. Zhang, W. Huang, *Adv. Mater.* **2014**, *26*, 7931; b) Y. Im, M. Kim, Y. J. Cho, J.-A. Seo, K. S. Yook, J. Y. Lee, *Chem. Mater.* **2017**, *29*, 1946; c) M. Y. Wong, E. Zysman-Colman, *Adv. Mater.* **2017**, *29*, 1605444; d) Z. Yang, Z. Mao, Z. Xie, Y. Zhang, S. Liu, J. Zhao, J. Xu, Z. Chi, M. P. Aldred, *Chem. Soc. Rev.* **2017**, *46*, 915; e) X. Cai, S. J. Su, *Adv. Funct. Mater.* **2018**, *28*, 1802558; f) Y. Liu, C. Li, Z. Ren, S. Yan, M. R. Bryce, *Nat. Rev. Mater.* **2018**, *3*, 18020; g) Y. Zou, S. Gong, G. Xie, C. Yang, *Adv. Opt. Mater.* **2018**, *6*, 1800568; h) X. Liang, Z.-L. Tu, Y.-X. Zheng, *Chem. - Eur. J.* **2019**, *25*, 5623.

[2] H. Uoyama, K. Goushi, K. Shizu, H. Nomura, C. Adachi, *Nature* **2012**, *492*, 234.

[3] a) W. Zeng, H. Y. Lai, W. K. Lee, M. Jiao, Y. J. Shiu, C. Zhong, S. Gong, T. Zhou, G. Xie, M. Sarma, K. T. Wong, C. C. Wu, C. Yang, *Adv. Mater.* **2017**, *30*, 1704961; b) Y. Yuan, Y. Hu, Y.-X. Zhang, J.-D. Lin, Y.-K. Wang, Z.-Q. Jiang, L.-S. Liao, S.-T. Lee, *Adv. Funct. Mater.* **2017**, *27*, 1700986; c) J.-X. Chen, K. Wang, C.-J. Zheng, M. Zhang, Y.-Z. Shi, S.-L. Tao, H. Lin, W. Liu, W.-W. Tao, X.-M. Ou, X.-H. Zhang, *Adv. Sci.* **2018**, *5*, 1800436; d) J.-X. Chen, W.-W. Tao, W.-C. Chen, Y.-F. Xiao, K. Wang, C. Cao, J. Yu, S. Li, F.-X. Geng, C. Adachi, C.-S. Lee, X.-H. Zhang, *Angew. Chem., Int. Ed.* **2019**, *58*, 14660; e) Y. Zhang, D. Zhang, T. Huang, A. J. Gillett, Y. Liu, D. Hu, L. Cui, Z. Bin, G. Li, J. Wei, *Angew. Chem., Int. Ed.* **2021**, *60*, 20498.

[4] a) T.-L. Wu, M.-J. Huang, C.-C. Lin, P.-Y. Huang, T.-Y. Chou, R.-W. Chen-Cheng, H.-W. Lin, R.-S. Liu, C.-H. Cheng, *Nat. Photonics* **2018**, *12*, 235; b) Y. Im, J. Y. Lee, *J. Inf. Disp.* **2017**, *18*, 101; c) Y. Zhang, D. Zhang, J. Wei, X. Hong, Y. Lu, D. Hu, G. Li, Z. Liu, Y. Chen, L. Duan, *Angew. Chem., Int. Ed.* **2020**, *132*, 17652.

[5] a) D. H. Ahn, S. W. Kim, H. Lee, I. J. Ko, D. Karthik, J. Y. Lee, J. H. Kwon, *Nat. Photonics* **2019**, *13*, 540; b) Y. Kondo, K. Yoshiura, S. Kitera, H. Nishi, S. Oda, H. Gotoh, Y. Sasada, M. Yanai, T. Hatakeyama, *Nat. Photonics* **2019**, *13*, 678; c) Q. Zhang, B. Li, S. Huang, H. Nomura, H. Tanaka, C. Adachi, *Nat. Photonics* **2014**, *8*, 326.

[6] Y. Xie, Z. Li, *J. Polym. Sci., Part A: Polym. Chem.* **2017**, *55*, 575.

[7] a) X.-K. Chen, S.-F. Zhang, J.-X. Fan, A.-M. Ren, *J. Phys. Chem. C* **2015**, *119*, 9728; b) J. Gibson, A. P. Monkman, T. J. Penfold, *ChemPhysChem* **2016**, *17*, 2956; c) J. Eng, J. Hagon, T. J. Penfold, *J. Mater. Chem. C* **2019**, *7*, 12942.

[8] a) K. Albrecht, K. Matsuoka, K. Fujita, K. Yamamoto, *Angew. Chem., Int. Ed.* **2015**, *54*, 5677; b) X. Ban, W. Jiang, T. Lu, X. Jing, Q. Tang, S. Huang, K. Sun, B. Huang, B. Lin, Y. Sun, *J. Mater. Chem. C* **2016**, *4*, 8810; c) Y. Li, G. Xie, S. Gong, K. Wu, C. Yang, *Chem. Sci.* **2016**, *7*, 5441; d) J. Luo, S. Gong, Y. Gu, T. Chen, Y. Li, C. Zhong, G. Xie, C. Yang, *J. Mater. Chem. C* **2016**, *4*, 2442; e) K. Albrecht, K. Matsuoka, D. Yokoyama, Y. Sakai, A. Nakayama, K. Fujita, K. Yamamoto, *Chem. Commun.* **2017**, *53*, 2439; f) X. Ban, W. Jiang, K. Sun, B. Lin, Y. Sun, *ACS Appl. Mater. Interfaces* **2017**, *9*, 7339; g) Y. Li, T. Chen, M. Huang, Y. Gu, S. Gong, G. Xie, C. Yang, *J. Mater. Chem. C* **2017**, *5*, 3480; h) M. Godumala, S. Choi, H. J. Kim, C. Lee, S. Park, J. S. Moon, K. S. Woo, J. H. Kwon, M. J. Cho, D. H. Choi, *J. Mater. Chem. C* **2018**, *6*, 1160; i) K. Matsuoka, K. Albrecht, A. Nakayama, K. Yamamoto, K. Fujita, *ACS Appl. Mater. Interfaces* **2018**, *10*, 33343.

[9] S. Hirata, Y. Sakai, K. Masui, H. Tanaka, S. Y. Lee, H. Nomura, N. Nakamura, M. Yasumatsu, H. Nakanotani, Q. Zhang, K. Shizu, H. Miyazaki, C. Adachi, *Nat. Mater.* **2015**, *14*, 330.

[10] K. Albrecht, K. Matsuoka, K. Fujita, K. Yamamoto, *Mater. Chem. Front.* **2018**, *2*, 1097.

[11] a) K. Sun, Y. Sun, D. Liu, Y. Feng, X. Zhang, Y. Sun, W. Jiang, *Dyes Pigm.* **2017**, *147*, 436; b) K. Sun, Y. Sun, W. Tian, D. Liu, Y. Feng, Y. Sun, W. Jiang, *J. Mater. Chem. C* **2018**, *6*, 43.

[12] a) T. Matulaitis, P. Imbrasas, N. A. Kukhta, P. Baronas, T. Bučiūnas, D. Banevičius, K. Kazlauskas, J. V. Gražulevičius, S. Juršėnas, *J. Phys. Chem. C* **2017**, *121*, 23618; b) R. Braveenth, K. Y. Chai, *Materials* **2019**, *12*, 2646.

[13] W.-L. Tsai, M.-H. Huang, W.-K. Lee, Y.-J. Hsu, K.-C. Pan, Y.-H. Huang, H.-C. Ting, M. Sarma, Y.-Y. Ho, H.-C. Hu, C.-C. Chen, M.-T. Lee, K.-T. Wong, C.-C. Wu, *Chem. Commun.* **2015**, *51*, 13662.

[14] H. Liu, J. Zeng, J. Guo, H. Nie, Z. Zhao, B. Z. Tang, *Angew. Chem., Int. Ed.* **2018**, *57*, 9290.

[15] Z. Huang, Z. Bin, R. Su, F. Yang, J. Lan, J. You, *Angew. Chem., Int. Ed.* **2020**, *59*, 9992.

[16] D. Liu, W. Tian, Y. Feng, X. Zhang, X. Ban, W. Jiang, Y. Sun, *ACS Appl. Mater. Interfaces* **2019**, *11*, 16737.

[17] T. Huang, W. Jiang, L. Duan, *J. Mater. Chem. C* **2018**, *6*, 5577.

[18] D. Sun, R. Saxena, X. Fan, S. Athanasopoulos, E. Duda, M. Zhang, S. Bagnich, X. Zhang, A. Köhler, E. Zysman-Colman, *Adv. Sci.* **2022**, https://doi.org/10.1002/advs.202201470.

[19] J. Gibson, T. Penfold, *Phys. Chem. Chem. Phys.* **2017**, *19*, 8428.

[20] A. M. Nardes, M. Kemerink, M. M. de Kok, E. Vinken, K. Maturova, R. A. J. Janssen, *Org. Electron.* **2008**, *9*, 727.

[21] E. Duda, D. Hall, S. Bagnich, C. L. Carpenter-Warren, R. Saxena, M. Y. Wong, D. B. Cordes, A. M. Z. Slawin, D. Beljonne, Y. Olivier, E. Zysman-Colman, A. Köhler, *J. Phys. Chem. B* **2022**, *126*, 552.

[22] P.-I. Shih, C.-L. Chiang, A. K. Dixit, C.-K. Chen, M.-C. Yuan, R.-Y. Lee, C.-T. Chen, E. W.-G. Diau, C.-F. Shu, *Org. Lett.* **2006**, *8*, 2799.

[23] G. Wypych, *Handbook of Solvents*, ChemTec Publishing, Toronto, Canada **2001**.

[24] a) H. Noda, X.-K. Chen, H. Nakanotani, T. Hosokai, M. Miyajima, N. Notsuka, Y. Kashima, J.-L. Brédas, C. Adachi, *Nat. Mater.* **2019**, *18*, 1084; b) L.-S. Cui, A. J. Gillett, S.-F. Zhang, H. Ye, Y. Liu, X.-K. Chen, Z.-S. Lin, E. W. Evans, W. K. Myers, T. K. Ronson, H. Nakanotani, S. Reineke, J.-L. Bredas, C. Adachi, R. H. Friend, *Nat. Photonics* **2020**, *14*, 636.